Formation, Structure, and Stability of Titanate Nanotubes and Their Proton Conductivity

Alistair Thorne,[†] Angela Kruth,[†] David Tunstall,[‡] John T. S. Irvine,*[,†] and Wuzong Zhou*[,†]

School of Chemistry and School of Physics and Astronomy, University of St. Andrews, St. Andrews, Fife KY16 9ST, United Kingdom

Received: July 1, 2004; In Final Form: November 10, 2004

High-yield H-form trititanate nanotubes have been synthesized, and their structures have been characterized by using X-ray diffraction and high-resolution transmission electron microscopy. According to combined TGA/XRD studies, the nanotubes are not stable at high temperature. Thermal analysis suggests that the stoichiometry of the material is $H_2Ti_3O_7 \cdot 0.8H_2O_{abs}$. Conductivity measurements indicate that mainly protonic transport occurs at temperatures below 150 °C and that with increasing temperature and progressive breakdown of nanotubes and formation of crystalline TiO_2 phases protonic conductivity is lost, leaving only residual defect electronic conduction. The proton conductivity is ca. 5.5×10^{-6} S cm^{-1} at 300 K. The structural protons and trapped water were confirmed by solid-state NMR.

I. Introduction

Since the discovery of carbon nanotubes[1] 13 years ago, this new form of material has attracted a great deal of attention from scientists and industrials because of its novel electronic and mechanical properties. In a short period of time, some inorganic oxide nanotubes were also developed.[2−5] Among them, titania nanotubes, first reported by Kasuga et al. five years ago,[4,5] are particularly interesting because of their crystalline and scroll structure. The material can be easily fabricated by treating crystalline TiO_2 with highly concentrated NaOH. According to the synthesis conditions used by Kasuga et al., washing the alkali-treated sample with water and further reaction with HCl are two crucial steps in the formation of titania nanotubes.[5] Later, Chen et al. reproduced the materials using a similar method and found that the nanotubes could be prepared via a single hydrothermal alkali treatment of any crystalline TiO_2.[6] Chiefly on the basis of powder X-ray diffraction (XRD) and high-resolution transmission electron microscopy (HRTEM), Chen et al. also proposed that the product is not titania as determined by Kasuga et al. and that the structure of the product can be regarded as rolled up individual layers derived from one of the $H_2Ti_3O_7$ structures with a C-centered monoclinic unit cell with $a = 1.603$, $b = 0.375$, $c = 0.919$ nm, and $\beta = 101.45°$.[7] However, the presence of protons in the interlayer space could not be detected by HRTEM and therefore remained uncertain.

Hydrogen titanate materials with a compostion of $H_2Ti_3O_7$ but with an alternative structure type (ramsdellite structure) were previously shown to exhibit attractive conductivities at low temperatures that are most likely due to protonic transport, which suggests a potential application of hydrogen titanates as fuel cell electrolytes in protonic fuel cells.[8]

In the present work, we tried to synthesize a high-yield and relatively pure specimen of trititanate nanotubes and investigated their physicochemical properties by various methods such as thermal analysis, ionic conductivity, and solid-state NMR. We then confirmed the $H_2Ti_3O_7$-type structure with a high content of protons.

II. Experimental Section

Synthesis of the specimen was by a modification of the previously reported method.[6] Rutile-type TiO_2 (7.9859 g (0.10 mol); 99.999%) was placed into a beaker (100 cm^3). Using a syringe, we added 10 M sodium hydroxide solution (2×10 cm^3 portions). The mixture was left stirring for 30 min. The resultant white slurry was transferred to a Teflon vessel, and more sodium hydroxide (3 cm^3) was used to wash out the remaining slurry. The Teflon vessel was placed into a sealed autoclave and put in an oven at 150 °C for 72 h. After cooling to room temperature, the solid white product was scraped out and filtered under reduced pressure. The product was placed into a conical flask with distilled water (150 cm^3), heated (50 °C, hotplate), and stirred vigorously for 30 min. The sample was then filtered under reduced pressure, and the pH of the filtrate was measured. Fresh distilled water (3×100 cm^3) was washed over the product. The product was then removed and stirred, with heating, for another 30 min followed by filtration. These steps were repeated until the pH was measured to be neutral. At this point, it was vacuum dried and transferred to an oven and dried to constant mass. Finally, the powder was washed with alternate 0.1 M HCl and distilled water in an ultrasonic bath for ca. 10 min. The powder and liquid were afterward separated by centrifuging.

Structural investigations were carried out using a combination of electron microscopy and powder XRD. Scanning electron microscopy (SEM) images were recorded on a JEOL JSM-5600 scanning electron microscope operated at an accelerating voltage of 20 kV. HRTEM images and selected area electron diffraction (SAED) patterns were recorded using a Gatan CCD camera on a JEOL JEM-2011 electron microscope operating at 200 kV. The chemical composition of the nanotubes was examined with energy-dispersive X-ray spectroscopy (EDX) using an Oxford Link system installed in the JEM-2011 microscope and an Oxford Inca system, which was integrated within the JSM-5600 microscope. Optimization of the instrument was carried out

* Corresponding authors. E-mail: jtsi@st-andrews.ac.uk, wzhou@st-andrews.ac.uk.
[†] School of Chemistry, University of St. Andrews.
[‡] School of Physics and Astronomy, University of St. Andrews.

10.1021/jp047113f CCC: $30.25
Published on Web 02/03/2005

using Co as an optimization element. Titanium metal and albite, $NaAlSi_3O_8$, were used as references for calibration. XRD was carried out using a STOE Stadi P transmission diffractometer over the 2θ range of 5 to 70°, step width 0.02° 2θ.

Thermal analysis was carried out on a RheoTherm TGA instrument. Heating of the TiO_2 nanotube powders was carried out at a heating rate of 5 °C/min from room temperature to temperatures up to 950 °C in static air. The samples were then held at maximum temperature for 15 min and subsequently cooled at a rate of 5 °C/min.

For conductivity studies, the nanotube powder was pressed into a pellet of ca. 10-mm diameter and 1.5-mm thickness using an axial pressure of ca. 9 MPa. Teflon (1%) was added to the powder as a binder. The pellet was then coated with a thin layer of Ag paint. ac impedance spectroscopy was carried out over the temperature range from room temperature to 300 °C, equilibrating for 1 h at each temperature, resulting in an average heating rate of ca. 30 °C/h. For this, the conductivity jig was inserted in a horizontal tube furnace, and data were collected in static air over a frequency range of $10^{-1}-10^{7}$ Hz using a Solartron 1250/1287 impedance analyzer. Data were not corrected for sample porosity.

The NMR experiments used single-pulse acquisition with pulses of about 45° (1 μs) generated in an Infinity Plus Varian 500-MHz spectrometer with a receiver delay of 5 μs and a bandwidth of 1 MHz. The pulse repetition frequency was 1 Hz, and the acquisition time was typically 10.024 ms. Signals were acquired as the average of four acquisitions. The experiments were undertaken with 4-mm zirconia rotors, Teflon spacers and end-caps, and vespel drive tips. Chemical shifts are referenced with respect to +1.3 ppm for the MAS proton peak of adamantane; this puts TMS at 0 ppm. The samples were spun and heated with dry nitrogen gas.

III. Results and Discussion

Synthesis Conditions. Although the synthetic method for the titanate nanotubes is relatively uncomplicated, the yield of the product mainly depends on the reaction time and temperature. To investigate the quantity of nanotubes produced under different reaction conditions, we carried out repeated experiments by varying the time and temperature of the reaction. We found that, under some conditions, the formation of nanotubes was accompanied by the formation of some byproducts such as amorphous phases, nanowires, nanofibers, and nanoplates. All of these materials give very weak signals in XRD; therefore, quantifying the nanotubes produced was done by a visual estimation of the percentage area presented by nanotubes in the TEM. When the reaction time of 72 h was fixed, it was found that about 35% nanotubes were produced when the reaction temperature was 130 °C. The yield increased to about 80% when the temperature was increased to 150 °C, and the value decreased to about 60% with a further increase in temperature to 170 °C. However, when the temperature was set to 150 °C, the yield of the nanotubes increased from zero to about 80% when reaction times of 2, 4, 8, 24, and 72 h were applied. The yield dropped sharply when the reaction time was further increased to 96 and 120 h. Consequently, a temperature of 150 °C and a reaction time of 72 h are about the optimum conditions required for the synthesis of the titanate nanotubes. The sample prepared under these conditions was then used in the further investigation.

The overall composition of the sample powder was analyzed by means of an EDX/SEM. EDX analysis was carried for Na and Ti from 15 different sample areas of 50 × 50 μm^2 using an acceleration voltage of 25 kV. It was observed that as-prepared samples contained large amounts of sodium (8:17 W_{Na}/W_{Ti}) (Figure 1a), although the pH of the parent filtrate was neutral and no sodium was detected by EDX/TEM from individual nanotubes. To remove the sodium impurities from the sample, the powder was washed several times alternatively with dilute HCl and H_2O, and after each HCl/H_2O treatment, the sodium content was analyzed. After two repeated HCl/H_2O washings, the sodium/titanium ratio was ca. 4:96, and after four repeated washings, no sodium was detected (Figure 1b). TEM was carried out on the sample after four repeated HCl/H_2O washings, and no degradation of the nanotubes was observed by TEM analysis.

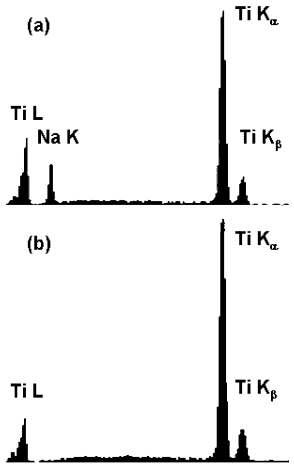

Figure 1. Large-area EDX analyses of the trititanate nanotubes: (a) sample before acid washing and (b) sample after four HCl/H_2O washing treatments.

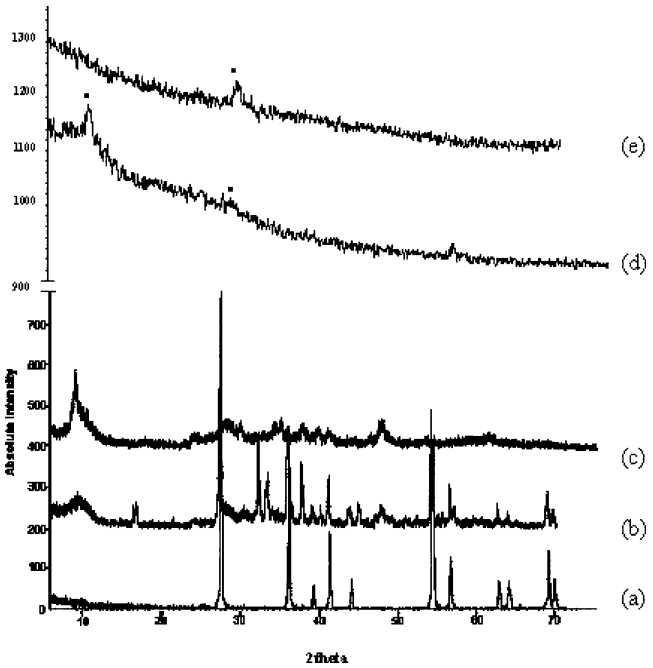

Figure 2. Powder XRD patterns of (a) the raw material, rutile TiO_2, (b) the product after 24 h of reaction at 150 °C, (c) the product after 72 h of reaction at 150 °C, and the product after (d) two and (e) four HCl/H_2O washing treatments.

XRD and Electron Microscopy. Powder XRD patterns for the starting material, rutile, and the progressive formation of the nanotubes are shown in Figure 2a−c, and the 2θ values of the diffraction peaks are listed in Table 1. The pattern for the sample after 24 h of reaction (b) shows all of the expected

TABLE 1: Comparison of Observed Reflections and Reflections Reported for an $A_2Ti_3O_7$-Type Compound

$A_2Ti_3O_7$ d(Å)/I_{rel}	2θ/deg	*hkl*	(b) 2θ/deg	(c) 2θ/deg	(d) 2θ/deg	(e) 2θ/deg
8.95/7	9.919	001				
7.82/100	11.306	200	9.58	9.17	10.80	
5.37/40	16.494	201	16.67			
			17.03			
4.48/6	19.801	002	21.25			
3.63/28	24.503	110	24.17	24.17		
			27.50[a]			
3.040/10	29.356	310	28.33	28.40		
2.998/32	29.777	003	30.42	30.00	29.17	30.67
2.783/7	32.137	311	32.08	33.12		
2.653/3	33.758	312	33.33	34.58		
2.482/16	36.161	602	36.25	35.86		
2.388/2	37.637	312	37.92	38.33		
2.366/4	38.000	113	39.17			
2.247/4	40.097	004	40.21	40.00		
			41.25	41.25		
2.055/20	44.029	204	43.75			
1.945/6	46.662	711	45.00			
		802				
1.869/11	48.679	020	48.33	48.33		

[a] Reflection corresponding to rutile TiO_2.

intense $A_2Ti_nO_{2n+1}$-type reflections but also indicates that the sample still contains significant amounts of crystalline rutile TiO_2. After 72 h of reaction time, no crystalline rutile TiO_2 was detected in the product (c), and a series of weak and broad diffraction peaks were observed that can be correlated to the $A_2Ti_nO_{2n+1}$ crystallographic series with $n = 3$ and A = H, Na.[7,9−12] We have noticed that the $A_2Ti_nO_{2n+1}$-type reflections in product (c) degrade in comparison with those in product (b). After removing the sodium from the sample by HCl/H_2O washing (Figure 2e), we observed no crystalline reflections except for a weak peak at ca. 30 2θ (d = 2.97 Å) that could correspond to the (003) reflection in $H_2Ti_3O_7$. These results suggest that patterns b, c, and d mostly originate from sodium titanate (Figure 2d) phases, $Na_2Ti_nO_{2n+1}$, and that the hydroxy titanate nanotube material has a significantly less ordered structure, especially within the interlayer spacings in the scroll; no crystalline phases such as anatase or rutile are present in the final product (Figure 2e).

The detailed structures of the nanotubes were examined using HRTEM. Figure 3 shows some typical HRTEM images of nanotubes in the final product. Figure 3a is an end-open nanotube with seven layers on one side and eight on the other. This is possible because the nanotube has a scroll structure as discussed in the previous report.[6] The measured interlayer spacing d is about 7.1 Å, corresponding to the d spacing of the (200) planes in $H_2Ti_3O_7$.

Figure 3b is an HRTEM image showing two nanotubes that are parallel and attached to one another. Measurement of the d spacing along the tube axis gives a value of 3.7 Å corresponding to the d spacing of the (010) planes in $H_2Ti_3O_7$, which is systematically absent in XRD. The (020) diffraction peak with a d spacing of 1.85 Å for the $H_2Ti_3O_7$ powder is very weak (Table 1), and it was not observed in the XRD pattern of the nanotubes. The d spacing along the direction perpendicular to the tube axis is about 2.9 Å, which is close to the value of the (003) planes in $H_2Ti_3O_7$. The corresponding XRD peak of these planes is the only one visible in the XRD pattern (Figure 2e). Consequently, the 2D lattice observed indicates that the nanotubes were formed by rolling a $Ti_3O_7^{2-}$ sheet, originally lying on the (011) plane in $H_2Ti_3O_7$, along the [001] direction.

Figure 3c is a nanotube that does not completely roll up. Although very thin plates with several $Ti_3O_7^{2-}$ sheets in

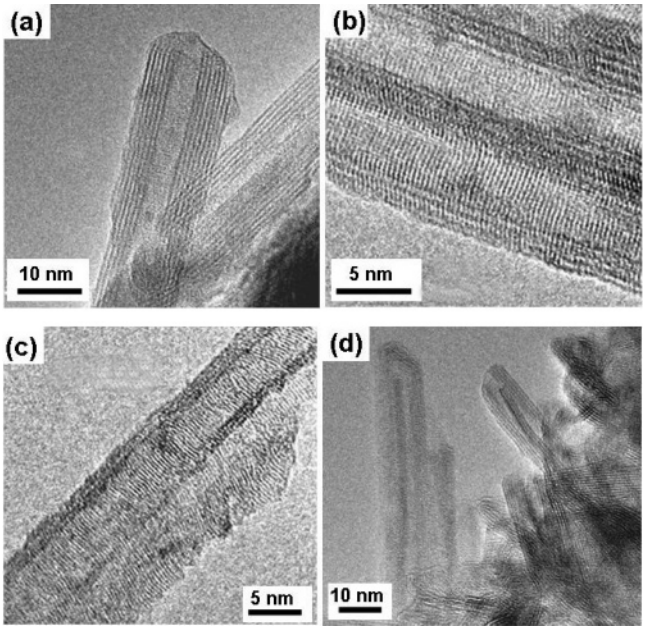

Figure 3. HRTEM images of the trititanate nanotubes showing (a) a single nanotube with seven layers on the left-hand side and eight layers on the right-hand side, (b) two parallel nanotubes attached to one another and with the 2D atomic lattice fringes confirming the rolling direction of the Ti−O sheets, (c) an incompletely rolled up nanotube, and (d) nanotubes that contain nanowires inside.

thickness were occasionally observed, the image in question is rare because the rolling process is governed by surface tension and must be very fast, according to a computer simulation.[13] The most likely reason for the termination of the rolling is the presence of structural defects in the $Ti_3O_7^{2-}$ sheet, releasing the surface tension.

Figure 3d shows some nanotubes with a solid nanowire inside the tubes. This could occur when the top Ti−O sheet is too small to form a nanotube and the second sheet underneath rolls up, enveloping the former inside the nanotube. It is worth noting that the length of the nanowires is similar to that of the nanotubes, and assuming they have a cylindrical shape, the diameter of these nanowires is only about 1.5 nm.

In addition, particle sizes of the raw material and the nanotube products were examined using SEM, and it was found that the dimensions of the nanotubes were independent of the particle size of TiO_2 crystals (about 200 nm). The above results confirmed the proposed formation mechanism: first TiO_2 reacts with NaOH to form an amorphous phase, which was observed only in specimens in the early stages of the reaction. Some multilayer $Na_2Ti_3O_7$-type sheets form in the amorphous phase, and individual layers of $Ti_3O_7^{2-}$ on the sheet surfaces roll up into nanotubes. The driving force of the rolling has been discussed by using a computer simulation method.[13] On washing with acid, the Na^+ ions are replaced by protons, decreasing the degree of crystallinity within the scroll.

An EDX/TEM examination of individual nanotubes indicated that there was no sodium in the nanotubes. However, the technique is not sensitive enough to detect hydrogen. This problem has been overcome by other experiments as discussed below.

Thermal Analysis. Powdered samples were heated at a constant rate to different temperatures (i.e., 150, 300, 600, and 900 °C) and subsequently cooled to room temperature. On heating, a weight loss of ΔW = 13 wt % occurred from 30 to ca. 500 °C. There is some evidence of an inflection in the weight trace in the range of 60−100 °C. (This inflection is present in

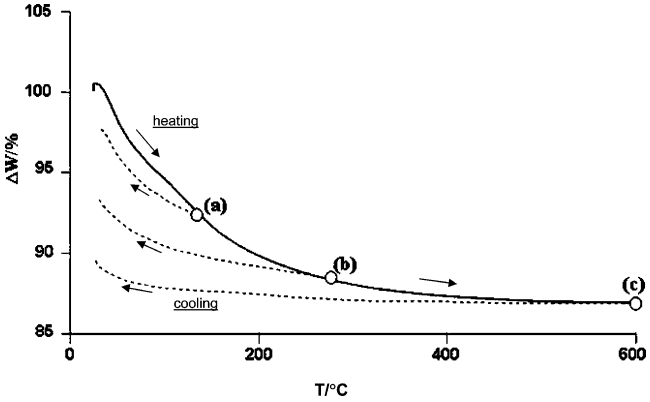

Figure 4. TGA traces of titanate nanotube material on heating in static air (solid line, all three experiments superimposed) and cooling in static air (dotted lines) for different maximum heating temperatures of (a) 150, (b) 300, and (c) 600 °C.

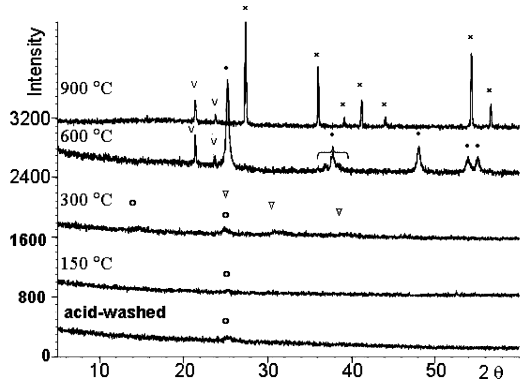

Figure 5. X-ray patterns for trititanate nanotube materials for the as-prepared and acid-washed samples and four samples that were heated to different temperatures (150, 300, 600, and 900 °C) during TGA experiments. Peaks correlate to nanotube material (○), TiO_2 brookite (▽), TiO_2 anastase (●), TiO_2 rutile (×), and vaseline from the sample holder (V).

all heating traces; see Figure 4.) ΔW is ca. 6% between 30 and 100 °C and ca. 7% on heating from 100 to 500 °C. No weight loss occurred at temperatures above 500 °C, confirming that all sodium was successfully removed from the material by the washing treatment. (Weight loss due to sodium loss has typically been observed at temperatures above 600 °C if the sample had been incompletely washed.) If the weight decrease is attributed entirely to water loss and it is assumed that no water is retained in the structure above 500 °C, then the TGA data suggest that the water content in the as-prepared sample is 0.615 mol of H_2O per TiO_2 formula unit (i.e., it has $H_{1.23}TiO_{2.62}$ stoichiometry). If the weight loss between 30 and 100 °C is attributed to the loss of water that was adsorbed at the surface and the weight loss between 100 and 500 °C is attributed to the loss of structural water, then the stoichiometry of the initial material is $H_{0.67}TiO_{2.33}\cdot 0.28H_2O_{abs}$ or $H_2Ti_3O_7\cdot 0.8H_2O_{abs}$. Accordingly, the stoichiometry of the TGA products after heating to temperatures of 150 and 300 °C was calculated to be $H_{0.19}TiO_{2.09}$ and $H_{0.57}TiO_{2.28}$, respectively. On cooling, all samples showed a small weight gain of 3−5% between 150 °C and room temperature. This weight gain most likely originates from the adsorption of moisture in static laboratory air.

All four products from thermal analysis (i.e., samples heated to 150, 300, 600, and 900 °C) were investigated by XRD and compared with that of the as-prepared sample (Figure 5). The as-prepared sample after washing, $H_{0.67}TiO_{2.33}\cdot 0.28H_2O_{abs}$ (or $H_2Ti_3O_7\cdot 0.8H_2O_{abs}$), and the sample that was heated to 150 °C with nominal composition, $H_{0.19}TiO_{2.09}$, showed little long-range order with just a small broad peak at 25° 2θ corresponding to the hydroxy titanate nanotubes (110 reflection in $A_2Ti_3O_7$). $H_{0.19}TiO_{2.09}$ was also analyzed by HRTEM, and it was observed that most of the nanotubes are still intact and only a small percentage of the nanotubes had decomposed. After heating to 300 °C and at nominal composition, $H_{0.57}TiO_{2.28}$, some additional broad peaks were observed at 30.3 and 39.5° 2θ, corresponding to d spacings of 2.95 and 2.28 Å, respectively. The most possible phase is TiO_2 brookite, and the observed peaks can be indexed as the (121) and (022) reflections from it. After heating to 600 °C, the material crystallized in the anatase structure, and at 900 °C, the rutile structure was formed.

From the TGA and XRD results, it can be concluded that the nanotubes are unstable on heating. Although the X-ray pattern at 300 °C could not be fully interpreted, additional peaks indicate that the formation of crystalline TiO_2 phases commence at this temperature or below. The nanotubes are likely to coexist with crystalline phases at low temperatures, but they are progressively destroyed on heating.

Conductivity. Stability studies have suggested that nanotubes are unstable on heating and that the formation of crystalline TiO_2 phases commences at temperatures $\leq$300 °C as a direct consequence of structural water loss. Conductivity studies were therefore carried out on a green nanotube pellet that was not subjected to thermal treatment prior to the measurement, with the addition of 1% Teflon as a binder. Ag electrodes were attached to the pellet by painting a Ag paste onto both of the parallel pellet faces. The paste was based on a solvent that readily evaporated at room temperature and therefore did not require firing of the electrodes.

The possibility of conductivity contributions from the Teflon binder was investigated by measuring the impedance response of a blank Teflon pellet with a geometry that was similar to that of the nanotube pellet and with Ag electrodes. Over the investigated temperature range, the Teflon pellet was observed to be highly resistive with $|Z| > 10^7\ \Omega$, even at 300 °C. It can be concluded that the contributions of Teflon to the total conductivity of the nanotube pellet must be comparably small and can be neglected.

The ac impedance response of a nanotube pellet was first measured on heating in air from room temperature to 300 °C. Figure 6 shows the complex impedance plane and the combined Z'', M'' spectroscopic plots at different temperatures (30, 90, and 300 °C) during the heating cycle. At least two contributions are apparent at 30 and 90 °C: a conductive high-frequency response, R_1C_1, and a resistive low-frequency response, R_2C_2. At 300 °C, the impedance complex plane consists of one semicircle only. The capacitance for the high-frequency response was $C_1 \approx 3-4$ pF cm^{-1} at 30 and 90 °C, and for the response at 300 °C, C_1 was $\sim$2 pF cm^{-1}. This suggests that the single contribution at 300 °C is equivalent to the R_1C_1 contribution at low temperatures and that it corresponds to the sample bulk. Spectroscopic plots show a relatively broad peak for R_1C_1 at 30 and 90 °C, but it is much sharper at high temperature, indicating a less distributed response at high temperature, perhaps due to a higher degree of crystallinity in the sample.

The Arrhenius plot of R_1C_1 conductivity values is shown in Figure 7. On heating, σ_1 increases from $\sigma_1 = 5.5 \times 10^{-6}$ S cm^{-1} at 30 °C to 1.5×10^{-5} S cm^{-1} at $T \approx 130$ °C. log σ_1 increases nonlinearly: there is a steady increase from 30 to 90 °C; however, on further heating, the increase with temperature occurs much more slowly. Above 130 °C, the conductivity drops drastically over 2 orders of magnitude to 5.6×10^{-8} S cm^{-1}

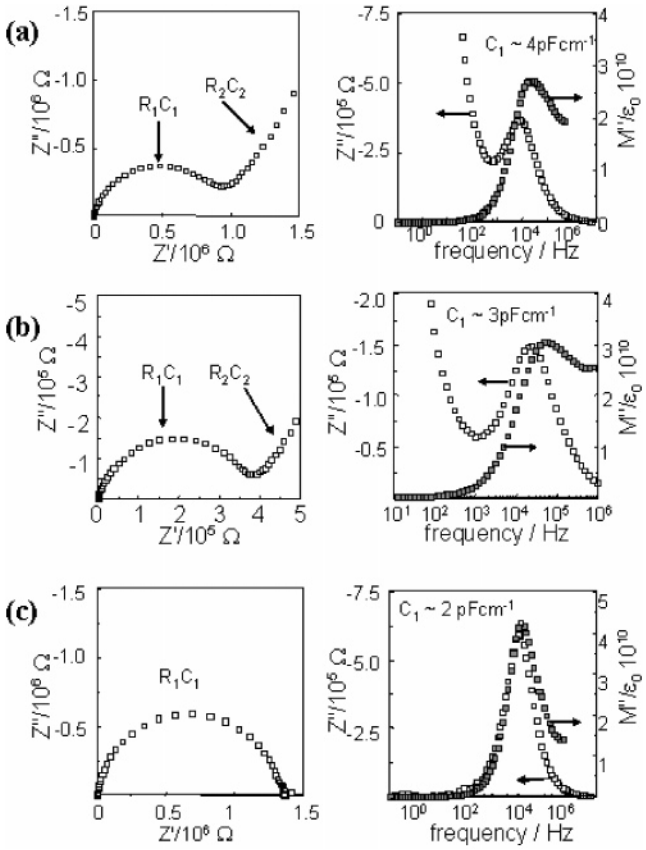

Figure 6. Complex impedance plane and combined Z'', M'' spectroscopic plots for a 99% titanate nanotube/1% Teflon pellet at (a) 30, (b) 90, and (c) 300 °C.

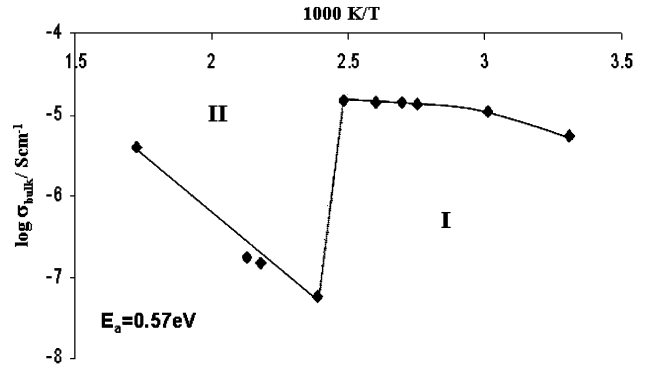

Figure 7. Arrhenius plot of bulk conductivities of trititanate nanotubes/Teflon with Ag electrodes on heating in static air.

at 150 °C. log σ_1 increases linearly on further heating with a calculated activation energy of $K_A = 0.57$ eV. The Arrhenius plot can therefore be divided into low-temperature and high-temperature parts, I and II. Conductivity values on cooling decreased linearly to $T \approx 160$ °C when the impedance values became too large to determine reliably. This suggests that the electrical character of the sample bulk changes on heating and that this change cannot be reversed on cooling. Clearly, the structural changes become irreversible in the temperature range of 130−150 °C. This is consistent with XRD data that show some evidence of the presence of a crystalline phase of TiO_2 (brookite) by 300 °C and TG analysis showing a much increased degree of irreversible water loss between 150 and 300 °C.

The bulk conductivity in region I must be dominated by protonic conduction in the nanotube material. On removal of water from the nanotubes during heating, the number of protons decreases, causing a deviation from a simple thermal activation process and hence a nonlinear increase of log σ_1 until at temperatures above 130 °C the protonic conduction pathway is disrupted and no significant long-range protonic conduction can occur. In region II, the conductivity is determined by the occurrence of electronic conduction with an activation energy of 0.57 eV. This value is slightly lower than the E_a obtained for electrical transport in nanoporous anastase and rutile materials, which was reported to be ca. 0.75−0.85 eV but is of similar order.[14] The loss of structural water is irreversible, and hence on cooling, electronic conductivity dominated.

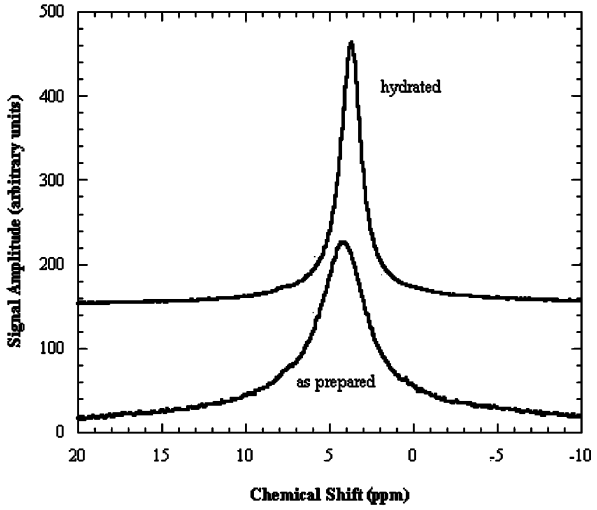

Figure 8. Two room-temperature spinning spectra for acid-washed nanotubes showing the contrast in line widths between as-prepared and hydrated samples.

Solid-State NMR. Two samples were used for the MAS NMR. The first is identical to the as-prepared sample that was alternately acid- and water-washed as described above. The second is identical to the first but was subjected to an extra thermal process by leaving it in a steam bath at 100 °C for several hours. Proton MAS NMR at 10 kHz was undertaken on both samples (Figure 8), and the second sample was subjected to an in situ temperature cycle to 180 °C in the NMR spectrometer with dry nitrogen gas.

Both samples produced simple one-line spectra at about 4.0 ppm relative to TMS, but the spectrum from the as-prepared sample was greater than 3 ppm in width whereas that from the thermally treated sample was only 1.5 ppm wide. The integrated peak intensity from the thermally treated sample was 2.3 times larger than that from the as-prepared sample. There were very small spinning sidebands in the spectrum of the thermally treated sample at room temperature but nothing in any of the other spectra at any temperature. An approximate estimate of the relative integrated intensity of the broad signal evidenced by the sidebands of the main central peak as shown in Figure 8 for this sample gives 20%. For both samples at room temperature, the static and 10-kHz spinning spectra were approximately the same, with the spinning spectrum in each case 20% narrower.

Dealing first with the as-prepared sample, with data only at room temperature, the position of the proton line reproduces the spectrum for water-washed nanotubes at room temperature, although the line is slightly broader, perhaps echoing the known extra disorder introduced by acid-washing. This is strong evidence that the line in the proton spectrum in this acid-washed sample is indeed due to structural protons in the nanotubes. There were no spinning sidebands for this acid-washed sample,

whereas the water-washed nanotubes did show significant sidebands; this probably indicates that trapped H_2O molecules are mobile at room temperature in acid-washed material

Turning now to the thermally treated sample, we find that the narrower line at room temperature (Figure 8) indicates an annealing feature of the treatment, restoring the line width to that observed in the water-washed nanotubes. The spinning sidebands indicate that there is some trapped immobile H_2O, and the extra proton intensity indicates that the hydrothermal treatment pushes more protons into the structure, although probably not in the form of H_2O because the TGA measurements indicate that at the temperature of the hydrothermal treatment, 100 °C, water is driven off. The temperature cycle to 180 °C in the thermally treated sample produced a significant loss in intensity with only small changes in the line width and line position for that line. After allowing for the normal Boltzmann decrease of the signal, we found that the integrated intensity decreased to 60% of its room-temperature value by 100 °C, after sitting at this temperature for 20 min, and to 25% when the temperature went up for another 20 min to 180 °C. This sample therefore has a substantial number of protons that are relatively easily detached, and these are not confined only to those protons that were added in the hydrothermal treatment. Small shifts in the peak position of the line as a result of the thermal treatment and with spinning are both consistent with the extra protons that are added by the thermal treatment being associated with the right-hand side (negative shift) of the NMR proton spectrum, indicating the difference between these protons and the structural protons, although their peaks are not resolvable.

In the acid-washed nanotubes, the structural protons and protons in any trapped water are not distinguishable by MAS NMR at room temperature in the as-prepared sample. By a thermal treatment protons can be added, and in this sample, trapped static water can be directly seen in the spinning sidebands. This and the thermal behavior of the peak position permits the assignment of the main peak in the spectrum of the as-prepared sample as predominantly due to structural protons; trapped water in this sample is mobile

In summary, conductivity measurement, thermoanalysis, and solid-state NMR investigation confirm that the nanotubes, produced by simple reaction of crystalline TiO_2 and highly concentrated NaOH, contain structural protons. The materials are H-form titanates rather than titania and decompose by dehydration below 300 °C. Structural characterizations by XRD and HRTEM further indicate that the structure of the nanotubes can be regarded as a result from rolling up individual sheets of $H_2Ti_3O_7$.

Acknowledgment. We thank SHEFC for financial support for the electron microscopy and solid state NMR facilities and EPSRC for a platform grant.

References and Notes

(1) Iijima, S. *Nature (London)* **1991**, *354*, 56.
(2) Satishkumar, B. C.; Govindaraj, A.; Vogl, E. M.; Basumallick, L.; Rao, C. N. R. *J. Mater. Res.* **1997**, *12*, 604.
(3) Niederberger, M.; Muhr, H.-J.; Krumeich, F.; Bieri, F.; Gunther, D.; Nesper, R. *Chem. Mater.* **2000**, *12*, 1995.
(4) Kasuga, T.; Hiramatsu, M.; Hoson, A.; Sekino, T.; Niihara, K. *Langmuir* **1998**, *14*, 3160.
(5) Kasuga, T.; Hiramatsu, M.; Hoson, A.; Sekino, T.; Niihara, K. *Adv. Mater.* **1999**, *11*, 1307.
(6) Chen, Q.; Zhou, W.; Du, G.; Peng, L.-M. *Adv. Mater.* **2002**, *14*, 1208.
(7) Feist, T. P.; Davies, P. K. *J. Solid State Chem.* **1992**, *101*, 275.
(8) Corcoran, D. J. D.; Tunstall, D. P.; Irvine, J. T. S. *Solid State Ionics* **2000**, *136*, 297.
(9) Nalbandyan, V.; Trubnikov, I. *Russ. J. Inorg. Chem.* **1987**, *32*, 639.
(10) Anderson, S.; Wadsley, A. D. *Acta Crystallogr.* **1961**, *14*, 1245.
(11) Dion, M.; Piffard Y.; Tournoux, M. *J. Inorg. Nucl. Chem.* **1978**, *40*, 917.
(12) Izawa, H.; Kikkawa, S.; Koizumi, M. *J. Phys. Chem.* **1982**, *86*, 5023.
(13) Zhang, S.; Peng, L.-M.; Chen, Q.; Du, G.; Dawson, G.; Zhou, W. *Phys. Rev. Lett.* **2003**, *91*, 256103.
(14) Dittrich, T.; Weidmann, J.; Timoshenko, V. Y.; Petrov, A. A.; Koch, F.; Lisachenko, M. G.; Lebedev, E. *Mater. Sci. Eng.* **2000**, *B69*, 489.